Inorg. Chem. **2007**, *46*, 710–719

The Copper(II) Adduct of the Unstructured Region of the Amyloidogenic Fragment Derived from the Human Prion Protein is Redox-Active at Physiological pH

Jason Shearer* and Pamela Soh

Department of Chemistry, University of Nevada at Reno, Reno, Nevada 89557

Received July 4, 2006

Prion diseases are caused by the misfolding and aggregation of the prion protein (PrP). Herein we provide evidence that the Cu^{II} adduct of the unstructured amyloidogenic fragment of the human PrP (PrP(91–126)) is redox active under physiological conditions. We have identified that the relevant high-affinity Cu^{II} binding region of PrP(91–126) is contained between residues 106 and 114. Both [Cu^{II}(PrP(91–126))] and [Cu^{II}(PrP(106–114))] have Cu^{II} K_d values of ~90 μM. Furthermore, the smaller PrP fragment PrP(106–114) coordinates Cu^{II} producing an electronic absorption spectrum nearly identical with [Cu^{II}(PrP(91–126))] (λ_{max} ~ 610 nm (ϵ ~ 125 M^{-1} cm^{-1})) suggesting a similar coordination environment for Cu^{II}. Cu K-edge X-ray absorption spectroscopy (XAS) reveals a nearly identical $CuN_{(N/O)_2}S$ coordination environment for these two metallopeptides (2N/O at ~1.97 Å; 1S at ~ 2.30 Å; 1 imidazole N at ~1.95 Å). Both display quasireversible Cu^{II}/Cu^{I} redox couples at ~–350 mV vs Ag/AgCl. ESI-MS indicates that both peptides will coordinate Cu^{I}. However, XAS indicates differential coordination environments between [Cu^{I}(PrP(91–126))] and [Cu^{I}(PrP(106–114))]. These data indicate that [Cu^{I}(PrP(91–126))] contains Cu in a four coordinate $(N/O)_2S_2$ environment with similar (N/O)–Cu bond distances (Cu–(N/O) r = 2.048(4) Å), while [Cu^{I}-(PrP(106–114))] contains Cu in a four coordinate $(N/O)_2S_2$ environment with differential (N/O)–Cu bond distances (Cu–(N/O) r_1 = 2.057(6) Å; r_2 = 2.159(3) Å). Despite the differential coordination environments both Cu-metallopeptides will catalytically reduce O_2 to $O_2^{\bullet-}$ at comparable rates.

Transmissible spongiform encephalopathies (prion diseases)[1,2] are fatal neurodegenerative disorders found in a number of organisms such as humans (Creutzfeldt−Jacobs disease and kuru), sheep and goats (scrapie), deer and elk (chronic wasting disease), and cattle (bovine spongiform encephalopathy or "mad cow").[3] It is thought that prion diseases are caused by the misfolding of the neuronal membrane prion protein (PrP) into its scrapie isoform (PrP^{Sc}).[1−3] PrP^{Sc} then aggregates into amyloid fibrils, forming plaques, which lead to neuron death. The mechanism of PrP misfolding is currently unknown, but it appears that exposure of PrP^{Sc} to the normally folded isoform will induce its misfolding. Other studies have shown that exposure of transgenic mice to smaller human PrP fragments, such as the unacylated unstructured fragment containing residues 106−126 (PrP(106−126); H_2N-KTNMKHMAGAAAAGAVVGGLG) can induce PrP aggregation leading to neuron death.[4]

Several parallels have been made between PrPs and the β-amyloid protein, which can aggregate into amyloid fibrils causing Alzheimer's disease.[5] One parallel both have an affinity for transition metal ions, including Cu^{II}.[5b,6,7] Several segments of the human PrP have been identified that possess a high affinity for Cu^{II}. The best characterized Cu^{II} binding domain is found between residues 60 and 91 (WGQ-$(PHGGGWGQ)_4$).[8] This segment, termed the octarepeat domain, can coordinate up to four Cu^{II} ions in a square planar/pyramidal Cu^{II} coordination geometry. Furthermore the affinity for Cu^{II} within the octarepeat domain is high,[8a,d]

* To whom correspondence should be addressed. E-mail: shearer@chem.unr.edu.

(1) Prusiner, S. B. *Science* **1982**, *216*, 136−144.
(2) Edkes, H. K; Wickner, R. B. *Nature* **2004**, *430*, 977−979.
(3) (a) Prusiner, S. B. *Proc. Natl. Acad. Sci. U.S.A.* **1998**, *95*, 13363−13383. (b) Castilla, J.; Saa, P.; Hetz, C.; Soto, C. *Cell* **2005**, *121*, 195−206. (c) Baylis, M.; Goldmann, W. *Curr. Mol. Med.* **2004**, *4*, 385−396. (d) Prusiner, S. B. *Science* **1997**, *278*, 245−251.
(4) Brown, D. R.; Schmidt, B.; Kretzschmar, H. A. *Nature* **1996**, *380*, 345−347.
(5) (a) Aguzzi, A.; Haass, C. *Science* **2003**, *302*, 814−819. (b) Gaggelli, E.; Kozlowski, H.; Valensin, D.; Valensin, G. *Chem. Rev.* **2006**, *106*, 1995−2044.
(6) Viles, J. H.; Cohen, F. E.; Prusiner, S. B.; Goodin, D. B.; Wright, P. E.; Dyson, J. H. *Proc. Natl. Acad. Sci. U.S.A.* **1999**, *96*, 2042−2047.
(7) Bush, A. I.; Masters, C. L. Tanzi, R. E. *Proc. Natl. Acad. Sci. U.S.A.* **2003**, *100*, 11193−11194.

10.1021/ic061236s CCC: $37.00
Published on Web 01/11/2007

and it has been shown that this region renders Cu^{II} in a redox-inactive state.[8c] Therefore, it has been speculated that the PrP may be involved in copper transport or homeostasis,[9] although the exact function of the PrP remains unknown.

Outside of the octarepeat domain a second segment of the human PrP has been identified that can coordinate Cu^{II}, the unstructured fragment PrP(91−126) (AcN-QGGGTH-SQWNKPSKPKTNMKHMAGAAAAGA VVGGLG).[8a,10] Cu coordination to PrP(91−126), which is disordered in solution when contained within the PrP, is not as well characterized as the octarepeat domain. Thus, the details concerning the physical and structural properties of its Cu^{II} adduct are debated.[11] It is still unknown if a CuN_4, CuN_3S, or other coordination mode is the physiologically relevant Cu-coordination mode within PrP(91−126).[8a,11] Furthermore, little is known about the Cu^{II} redox properties associated with this fragment.

In Alzheimer's disease many different mechanisms for neurodegeneration have been proposed; one proposal involves an oxidative stress type mechanism via the production of reactive oxygen species from a Cu^{II} β-amyloid adduct.[5b,7] Such a mechanism for prion diseases has been largely dismissed since it has been assumed that the PrP sequesters Cu^{II} in a redox-inactive state.[8a,c] However, the redox inactivity of Cu^{II} adducts of the PrP have been largely based on studies involving the octarepeat domain[8c] and not the amyloidogenic fragment. The speculation regarding the redox inactivity of the Cu (or other transition metal) adduct of the PrP also seems to be at odds with studies suggesting that metal adducts of the PrP can act as a superoxide dismutase or the findings that they can produce reactive oxygen species such as $HO^{\bullet}$, $O_2^{\bullet-}$, and H_2O_2.[12a−d] Furthermore, coordination of copper to PrP fragments have been shown to induce PrP aggregation.[12e,f] Also, the Cu^{II} adduct of PrP(92−96) appears to display redox activity.[12g] In this study we explore the structure of the Cu^{II} and Cu^{I} adduct the of PrP(91−126) as well as those of a smaller structural mimic, [$Cu^{II/I}$(PrP(106−114))] (PrP(106−114); AcN-KTNMKHMAG). We will show that these fragments are in fact redox active at physiological pH and are capable of producing $O_2^{\bullet-}$ in solution.

Experimental Section

Peptide Synthesis and Purification. All Novabiochem resins and Fmoc-protected amino acids were purchased from EMD Biosciences, while all other reagents were obtained from Fisher/Acros, were of the highest purity available, and used as received. Peptides were prepared using standard Fmoc based solid-phase chemistry using HOBt/HBTU/DIPEA[13] coupling strategies on Wang resin. Couplings were carried out either manually in a solid-phase reactor or automated using a Protein Technologies PS3 automated peptide synthesizer. Following cleavage from the resin (using 82.5% TFA, 2.5% EDT, 5% water, 5% thioanisol, and 5% phenol) the crude peptides were purified by preparative reverse phase HPLC followed by lyophilization. Analytical and preparative HPLC was performed on a Waters DeltaPrep 60 using Waters X-Terra C-18 columns (analytical, 5 μm and 4.6 × 100 mm; preparative, 5 μm and 50 × 100 mm). HPLC chromatograms were acquired under a positive pressure of He. All aqueous solutions were made from ultrapure water (>17.8 MΩ). ESI-MS data were recorded on a Waters Micromass 20 ESI mass spectrometer (positive ion mode). Gel permeation chromatography (GPC) was performed on a Waters DeltaPrep 60 equipped with a Protein-Pak GPC column (7.8 × 300 mm; 60 Å pore size) using water buffered to pH 7.4 (5 mM *N*-ethylmorpholine; NEM) under a positive pressure of He. GPC calibrations were made using a Waters polyethylene glycol standard kit.

AcN-QGGGTHSQWNKPSKPKTNMKHMAGAAAA-GAVVGGLG (PrP(91−126)). Gradient: 10−65% MeCN (0.1% TFA) in H_2O (0.1% TFA) over 45 min (preparative, 40 mL/min R_t = 29 min; analytical, 1 mL/min R_t = 31.3 min). Yield: ∼5%. **(**M)$^+$ (*m*/*z*): calcd, 3545.0; found, 3546.3.

AcN-KTNMKHMAG (PrP(106−114)). Gradient: 10−65% MeCN (0.1% TFA) in H_2O (0.1% TFA) over 45 min (preparative, 40 mL/min R_t = 3.2 min; analytical, 1 mL/min R_t = 3.7 min). Yield: 67%. (M)$^+$ (*m*/*z*): calcd, 1059.2; found, 1059.4.

Electronic Absorption Spectra of Cu-Metallopeptides and NBT/Formazan Assay for Superoxide. Electronic absorption studies were performed on a Varian CARY 50 UV/vis−NIR spectrophotometer using 1 cm quartz cuvettes. Peptide concentrations were either determined using the extinction coefficient of the W residue (ϵ_{280} = 5690 M^{-1} cm^{-1}) contained within the peptide (PrP(91−126)) or by preparing solutions from preweighed peptide and estimating a water content of ∼20% weight by weight of the lyophilized peptide (based on analogy to the W studies from above; PrP(106−114)). All peptide solutions were made using a 50 mM

(8) (a) Millhauser, G. L. *Acc. Chem. Res.* **2004**, *37*, 79−85. (b) Chattopadhyay, M.; Walter, E. D.; Newell, D. J.; Jackson, P. J.; Aronoff-Spencer, E.; Peisach, J.; Grefen, G. J.; Bennett, B.; Antholine, W. E.; Millhauser, G. L. *J. Am. Chem. Soc.* **2005**, *127*, 12647−12656. (c) Bonomo, R. P.; Impellizzeri, G.; Pappalardo, G.; Rizzarelli, E.; Tabbi, G. *Chem.*—Eur. J. **2000**, *6*, 4196−4202. (d) Jackson, G. S.; Murray, I.; Hosszu, L. L. P.; Waltho, J. P.; Clarke, A. R.; Collinge, J. *Proc. Natl. Acad. Sci. U.S.A.* **2001**, *98*, 8531−8535.

(9) Jones, C. E.; Klewpatinond, M.; Abdelraheim, S. R.; Brown, D. R.; Viles, J. H. *J. Mol. Biol.* **2005**, *346*, 1393−1407.

(10) (a) Hasnian, S. S.; Murphy, L. M.; Strange, R. W.; Grossmann, J. G.; Clarke, A. R.; Jackson, G. S.; Collinge, J. *J. Mol. Biol.* **2001**, *311*, 467−473. (b) Di Natale, G.; Grasso, G.; Impellizzeri, G.; La Mendola, D.; Micera, G.; Mihala, N.; Nagy, Z.; ¯Osz, K.; Pappalardo, G.; Rigó, V.; Rizzarelli, E.; Sanna, D.; Sóvágó, I. *Inorg. Chem.* **2005**, *44*, 7214−7215. (c) Burns, C. S.; Arnooff-Spencer, E.; Legname, G.; Prusiner, S. B.; Antholine, W. E.; Gerfen, G. J.; Peisach, J. Millhauser, G. L. *Biochemistry*, **2003**, *42*, 6794−6803. (d) Jones, C. E.; Abdelraheim, S. R.; Brown, D. R.; Viles, J. H. *J. Biol. Chem.* **2004**, *279*, 32018−32027.

(11) (a) Viles, J. H.; Cohen, F. E.; Prusiner, S. B.; Goodin, D. B.; Wright, P. E.; Dyson, J. H. *Proc. Natl. Acad. Sci. U.S.A.* **1999**, *96*, 2042−2047. (b) Brown, D. R.; Qin. K.; Herms, J. W.; Madlung, A.; Manson, J.; Strome, R. Fraser P. E.; Kruck T.; vonBohlen A.; Schulz-Schaeffer W.; Giese A.; Westaway D.; Kretzschmar H. *Nature* **1997**, *390*, 684−687. (c) Pauly, P. C.; Harris, D. A. *J. Biol. Chem.* **1998**, *273*, 33107−33110.

(12) (a) Brown, D. R.; Wong, B. S.; Hafiz, F.; Clive, C.; Haswell, S. J.; Jones, I. M. *Biochem. J.* **1999**, *344*, 1−5. (b) Turnbull, S.; Tabner, B. J.; Brown, D. R., Allsop, D. *Biochemistry*, **2003**, *42*, 7675−7681. (c) Turnbull, S.; Tabner, B. J.; Brown, D. R.; Allsop, D. *Neurosci. Lett.* **2003**, *336*, 159. (d) Madhavaiah, C.; Verma, S. *Bioorg. Med. Chem.* **2005**, *13*, 3241−3248. (e) Jobling, M. F.; Huang, X.; Stewart, L. R.; Barnham, K. J.; Curtain, C.; Volitakis, I.; Perugini, M.; White, A. R.; Cherny, R. A.; Masters, C. L.; Barrow, C. J.; Collins, S. J.; Bush, A. I.; Cappai, R. *Biochemistry* **2001**, *40*, 8073−8084. (f) Bocharova, O. V.; Breydo, L.; Salnikov, V. V.; Baskakov, I. V. *Biochemistry* **2005**, *44*, 6776−6787. (g) Hureau, C.; Charlet, L.; Dorlet, P.; Gonnet, F.; Spandini, L.; Anxolabéhère-Mallart, E.; Girerd, J-.J. *J. Biol. Inorg. Chem.* **2006**, *11*, 735−744.

(13) NBT: *para*-nitro-blue-tetrazolium chloride. HOBt: 1-hydroxybenotriazole. HBTU: *N*-[(1*H*-benzotriazol-1-yl)(dimethylamino)methylene]-*N*-methylmethanaminium hexaflurophosphate *N*-oxide. DIPEA: *N*,*N*-diisopropylethylamine. PrP(61−65.): AcN-HGGGW.

NEM solution buffered to pH = 7.4. Cu^{II} was added to the peptide solutions from a freshly prepared solution of $CuCl_2 \cdot 2H_2O$ (pH ~ 6.0). The Cu^{II} solution was fairly concentrated, and thus, the small quantity of Cu^{II} solution added did not have any measurable influence on the pH of the peptide solution. CD spectra were obtained on an OLIS DSM-17 spectropolarimeter. $O_2^{\bullet -}$ production was quantified using nitroblue tetrazolium (NBT). In a typical experiment a solution containing 0.50 mM [Cu^{II}(PrP(106−114))], 100 mM ascorbic acid, and 0.035 mM NBT was prepared (pH = 7.4). The electronic absorption spectrum was collected every 0.5 h (following gentle shaking by hand to resuspend any precipitated formazan) for 4 h monitoring the increase in a broad charge-transfer band centered at ~580 nm indicating the production of formazan.

XAS Data Measurement and Analysis. Freshly prepared solutions of $CuCl_2 \cdot 2H_2O$ in 50 mM NEM (pH 7.4) were added to solutions of the peptides in 50 mM NEM (pH 7.4). To ensure that only the high affinity copper site would be observed, we utilized an excess of peptide to Cu^{II} (1.0:0.8 ratio). The Cu^{I} peptides were prepared in an analogous manner in a glovebox under dinitrogen except, following $CuCl_2$ addition, an excess (~1.5 equiv) of ascorbic acid was added to solution. The copper-containing peptide solutions were then injected into aluminum sample holders in between two windows made of Kapton tape (cat. no. 1205; 3M, Minneapolis, MN) and quickly frozen in liquid nitrogen. Data were then collected at the National Synchrotron Light Source (Brookhaven National Laboratories, Upton, NY) on beamline X9b (ring operating conditions: 2.8 GeV; 200−305 mA). A focused Si(111) double monochromator was used for energy selection along with a low-angle Ni mirror for harmonic rejection. Energy calibrations were performed by recording a reference spectrum of Cu foil (first inflection point assigned to 8980.3 eV) simultaneously with the samples. All samples were maintained at 20 K throughout the data collection using a helium Displex cryostat. The spectra are reported as fluorescence data, which were recorded utilizing a 13-element Ge solid-state fluorescence detector (Canberra). Total count rates were maintained under 40 kHz per channel, and a deadtime correction of 3 μs was utilized (this had a negligible influence on the data). For XANES spectra the primary hutch aperture height was set to 0.4 mm to obtain the maximum resolution (theoretical maximum is ~0.9 eV) and data were obtained in 10 eV steps in the preedge region (8779−8958 eV), 0.3 eV steps in the edge region (8959−9023 eV), and 2.0 eV steps in the near-edge region. For EXAFS spectra the primary hutch aperture was set to 0.8 mm and data were obtained in 5.0 eV steps in the preedge region (8779−8958 eV), 0.5 eV steps in the edge region (8959−9023 eV), 2.0 eV steps in the near-edge region (9024−9278 eV), and 5.0 eV steps in the far-edge region (9279 eV−15.5 k). All spectra represent the averaged sum of at least 9 to as many as 15 spectra.

Data analysis was performed using the XAS analysis package EXAFS123,[14a] which consists of a series of macros and procedures written for the data analysis and graphing package Igor Pro (Wavemetrics; Lake Oswego, OR). EXAFS data were simulated using the single scatterer approximation:

$$\chi_{sim} = \sum_{i=1}^{\text{no. of shells}} n_i f_i k_i^{-1} r_i^{-2} \exp(-2\sigma^2 k_i^2) \sin(2k_i r_i + \alpha_i) \quad (1)$$

Here n_i is the number of scatterers in shell i, r_i is the distance the scatterer is from the absorber atom, σ^2 is the disorder factor, f_i is the amplitude function, α_i is the phase function, and k_i is defined as

$$k_i = 2\pi[2m_e(E - E_o)]^{1/2}/h \quad (2)$$

where E is the energy of the photon and E_o is energy at which EXAFS occurs. E_o was kept constant for all shells within the same metallopeptide but allowed to vary from metallopeptide to metallopeptide.

Phase and amplitude functions describing single scattering (SS) pathways for Cu−N, Cu−O, Cu−C, and Cu−S vectors were constructed using FEFF version 7.02[14b] as previously described.[14c] Multiple scattering pathways for the imidazole ring (Im) were constructed in a manner similar to that previously described by Scarrow et al.[14c] Briefly, appropriate atomic potentials and phase shifts were calculated for an idealized geometry of [Cu(PrP(109−112)] within FEFF 7.02 (see Supporting Information). The Cu−Im moiety (hydrogens removed) was then isolated from the other atoms in the FEFF simulation by placing the other atoms at a distance of ~50 Å from the Cu center. We chose to fix the imidazole ring geometries using the following values (N_1 is bound to copper). Bond lengths: N_1-C_2, 1.31 Å; N_1-C_5, 1.38 Å; C_2-N_3, 1.35 Å; N_3-C_4, 1.37 Å; C_4-C_5, 1.35 Å. Bond angles: N_1, 106°; C_2, 112°; N_3, 106°; C_4, 104°; C_5, 111°.[14d] From this we then varied three structural parameters: the $Cu-N_1$ bond length (r' varied between 1.7 and 2.3 Å); the $Cu-N_1-C_2$ bond angle (ϕ varied between 110 and 150°); the bond angle between the Cu and the mean plane of the Im ring (θ varied between a 0 and 40° deviation from planarity).

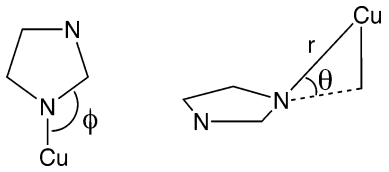

Although larger values for θ could be envisioned, these do not appear to contribute significantly to multiple scattering effects from the Cu−Im ring, and scattering from the ring could be simulated using Cu−C and Cu−N SS pathways. It was determined that depending on the bond length and angles between 14 and 38 pathways could contribute significantly to the Cu−Im spectrum. Instead of utilizing only the common MS pathways (which represented only a fraction of the total MS pathways from any one geometry), we chose to create a function for the whole Cu−Im moiety using the chi.dat output files from 48 reference spectra generated in FEFF 7.02. The chi.dat file contains phase and amplitude information for each of the simulated spectra. Parametrized α_{CuIm} and f_{CuIm} functions were then generated from this data as previously described using the following functional form, which gave excellent reproductions of simulated EXAFS data:

$$F_{CuIm} = F_0 + r'F_1 + \theta F_2 + \theta^2 F_3 + \phi^2 F_4 \quad (3)$$

$$F = \alpha \text{ or } f$$

Best fits to the experimental data were determined by selecting the model that gave both chemically reasonable refinement parameters

(14) (a) Scarrow, R. C. *EXAFS123*; Haverford College: Haverford, PA, 2005 (www.haverford.edu/chem/Scarrow/EXAFS123/). (b) Zabinsky, S. I.; Rehr, J. J.; Ankudinov, A.; Albers, R. C.; Eller, M. J. *Phys. Rev. B* **1995**, *52*, 2992−3009. (c) Scarrow, R. C.; Strickler, B. S.; Ellison, J. J.; Shoner, S. C.; Kovacs, J. A.; Cummings, J. G.; Nelson, M. J. *J. Am. Chem. Soc.* **1998**, *120*, 9237−9245. (d) Scarrow, R. C.; Brennan, B. A.; Cummings, J. G.; Jin, H.; Duong, D. J.; Kindt, J. T.; Nelson, M. *J. Biochemistry* **1996**, *35*, 10078−10088.

and the lowest value for the goodness of fit parameter:

$$\mathrm{GOF} = \mathrm{average}[(\chi - \chi_{\mathrm{sim}}\}/\mathrm{esd}_{\mathrm{data}}](n_i/(n_i - n_p))^{1/2} \quad (4)$$

Here n_i is the number of independent data points and n_p is the number of parameters used in the data simulations. All EXAFS refinements reported herein were performed on unfiltered $k^3(\chi)$ data over the range of $k = 2.2-14.3$ Å^{-1} for [Cu^{II}(PrP(106−114))] and $k = 2.2-12.0$ Å^{-1} for [Cu^{II}(PrP(91−126))].

The bond valence sum analysis[15] on all refined EXAFS models was applied according to

$$s_i = \exp[(r_o - r)/0.37] \quad (5)$$

$$\mathrm{BVS} = \sum_{i=1}^{n} s_i \quad (6)$$

where r is the experimentally derived bond length for ligand i and r_o is the reference bond length. The values used for r_o include $r_{\mathrm{Cu(II)S}} = 2.054$ Å, $r_{\mathrm{Cu(II)N}} = 1.751$ Å, $r_{\mathrm{Cu(II)O}} = 1.679$ Å, $r_{\mathrm{Cu(I)S}} = 1.898$ Å, $r_{\mathrm{Cu(I)N}} = 1.595$ Å, and $r_{\mathrm{Cu(I)O}} = 1.519$ Å.

Electrochemical Measurements. Electrochemical measurements were performed on a Princeton Applied Research PARSTAT 2273 potentiostat in a Faraday cage to minimize noise in the voltammograms. We utilized a glass cell with a solution containing NaCl (100 mM) at a pH = 7.4 (10 mM NEM buffer). Unless otherwise stated the solutions were continually sparged with Ar prior to data collection and maintained under a positive pressure of Ar during data collection. We utilized a three-electrode cell with a Ag/AgCl reference electrode, a Pt wire auxiliary electrode, and a Pt disk working electrode ($A = 0.2$ cm^2). The procedure of Rusling et al.[16] was used to apply the thin peptide films within a surfactant bilayer to the electrode surface as follows. An *N*,*N*-dimethyldidodecylammonium bromide (DDAB) bilayer was made by applying 10 μL of a 0.1 M solution of DDAB in chloroform to the freshly polished electrode surface. A small evaporation chamber was then placed over the electrode surface, and the chloroform was allowed to slowly evaporated overnight. A 0.5 mM metallopeptide solution (pH = 7.4, 50 mM NEM buffer) was then prepared and the electrode placed in this solution for ∼30 min by which time the metallopeptide had been incorporated into the bilayer. Cyclic (0.001−50 V s^{-1}) and square-wave (50−200 V s^{-1}) voltammograms were then collected for these metallopeptide films. The background current was subtracted from the data by fitting a cubic spline function to the baseline on each side of the peak. Standard rates for electron transfer (k_o) were then determined by

$$E_{\mathrm{pc}} = E^{\circ} - \frac{2.303RT}{\alpha nF}\log\frac{\alpha nF}{RTk_o} - \frac{2.303RT}{\alpha nF}\log v \quad (7)$$

$$E_{\mathrm{pa}} = E^{\circ} + \frac{2.303RT}{(1-\alpha)nF}\log\frac{(1-\alpha)nF}{RTk_o} + \frac{2.303RT}{(1-\alpha)nF}\log v \quad (8)$$

where α is the electron-transfer coefficient and the rest of the terms have their usual meaning.[17,18] The following parameters were set as constants: $E^{\circ} = -0.33$ V vs Ag/AgCl; $T = 300$ K; $n = 1$ e$^-$. The parameter α was originally allowed to refine and was then restrained to 0.59.

Determination of Cu^{II} Stability Constants for [Cu^{II}(PrP(91−126))] and [Cu^{II}(PrP(106−114))]. Stability constants for the metallopeptides were determined by fluorimetry on a Horiba Fluoromax-3 flourometer at a pH = 7.4 (50 mM NEM). We monitored the quenching of the W emission in PrP(91−126) at 350 nm following excitation at a wavelength of 285 nm. To determine the stability constant for [Cu^{II}(PrP(91−126))] a 5 μM metallopeptide solution was prepared (pH 7.4) and glycine was added to solution. The fluorescence intensity of the W emission at 350 nm for [Cu^{II}(PrP(91−126))] is 62% that of free PrP(91−126). As the glycine removes Cu^{II} from PrP(91−126) the W fluorescence increases in intensity until it reaches the intensity of free PrP(91−126). Concentration for all species present were then extracted at the midpoint of the glycine titration. The dissociation constant (K_d) for [Cu^{II}(PrP(91−126))] can be calculated according to

$$K_d = \beta^{-1}{K_{ex}}^{-1} \quad (9)$$

where

$${K_{ex}}^{-1} = \frac{[\mathrm{Cu^{II}(gly)_2}][\mathrm{PrP(91-126)}]}{[\mathrm{Cu^{II}(PrP(91-126))}][\mathrm{gly}]^2} \quad (10)$$

and the value for β for glycine at pH 7.4 is 7.08×10^5 M^{-1}.[19] Cu^{II} dissociation constants for [Cu^{II}(PrP(106−114))], which lacks a W residue, were obtained as outlined above except PrP(106−114) was used as a competitive Cu^{II} ligand in place of glycine once the formation constant for [Cu^{II}(PrP(91−126))] was known. Equation 10 had to then be modified to account for the fact PrP(106−114) forms a 1:1 adduct with Cu^{II} and not a 2:1 adduct as glycine does.

Results and Discussion

Cu^{II} Coordination to PrP(106−114) and PrP(91−126). There has been considerable debate concerning the identity of the physiologically relevant high-affinity Cu^{II} binding sequence within PrP(91−126). Therefore, we prepared several small peptide fragments found within PrP(91−126) to elucidate the minimal PrP sequence that affords Cu^{II} a coordination microenvironment similar to that of the full length fragment. As a quick initial probe for discerning similarities in Cu^{II} coordination environments electronic absorption spectroscopy was utilized focusing on the ligand-field bands centered between 400 and 900 nm. In these experiments 1 equiv of $CuCl_2$ was added to the PrP fragments at physiological pH (pH = 7.4; 50 mM *N*-ethylmorpholine buffer (NEM)). Coordination of 1 equiv of Cu^{II} to PrP(106−114) produced an electronic absorption spectrum with a broad transition in the visible region of the spectrum ($\lambda_{\mathrm{max}} = 613$ nm ($\epsilon = 117$ M^{-1} cm^{-1}); Figure 1). This is consistent with the reported electronic absorption spectrum of [Cu^{II}(PrP(106−114))] recently reported by Di Natale et al. in which it was demonstrated that Cu^{II} was fully coordinated to PrP-

(15) (a) Brown, I. D.; Altermatt, D. *Acta Crystallogr., Sect. B* **1985**, *41*, 244−247. (b) Thorp, H. H. *Inorg. Chem.* **1992**, *31*, 1585−1586.
(16) Rusling, J. F.; Nassar, A.-E. F. *J. Am. Chem. Soc.* **1993**, *115*, 11891−11897.
(17) Bard, A. J.; Faulkner, L. R. *Electrochemical Methods: Fundamentals and Applications*, 2nd ed.; John Wiley & Sons: New York, 2001.
(18) (a) Laviron, E. *J. Electroanal. Chem.* **1979**, *101*, 19−28. (b) Huang, X.-J.; Im, H.-S.; Yarimaga, O.; Kim, J.-H.; Jang, S.-Y.; Lee, D.-H.; Kim, H.-S.; Choi, Y.-K. *J. Electroanal. Chem.* **2006**, *594*, 27−34.
(19) (a) Dawson, R. M. C.; Elliot, D. C.; Elliot, W. H.; Jones, K. M. *Data for Biochemical Research*; Clarendon Press: Oxford, U.K., 1986. (b) Syme, C. D.; Nadal, R. C.; Rigby, S. E. J.; Viles, J. H. *J. Biol. Chem.* **2004**, *279*, 18169−18177.
(20) We note that Jackson et al.[8d] has reported a Cu^{II} K_d of $\sim 4 \times 10^{-14}$ M for PrP(91−231) at pH 8.0l however, many of the K_d values reported in that study are several orders of magnitude smaller than the K_d value reported by others.

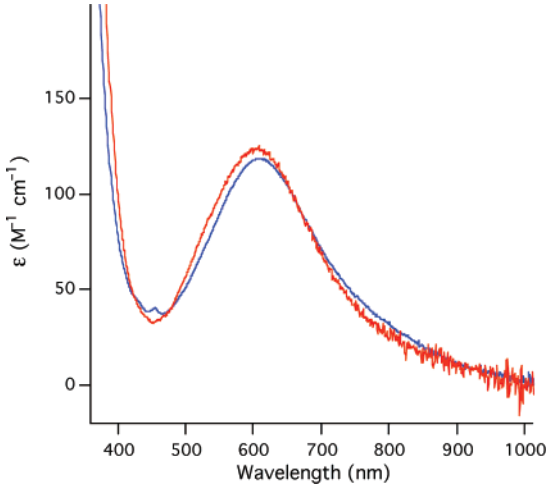

Figure 1. Electronic absorption spectra of [Cu^{II}(PrP(106−114))] (blue) and [Cu^{II}(PrP(91−126))] (red) recorded in 50 mM NEM (pH = 7.4).

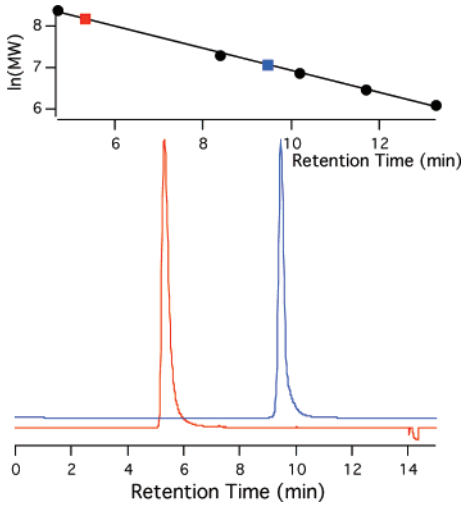

Figure 2. Gel permeation chromatogram (bottom) for [Cu^{II}(PrP(91−126))] (red) and [Cu^{II}(PrP(106−114))] (blue) recorded at a wavelength of 350 nm. The top shows the retention times of individual standards (black circles), the calibration curve (black line), and where [Cu^{II}(PrP(91−126))] (red square) and [Cu^{II}(PrP(106−114))] (blue square) fall on the calibration curve.

(106−114) at physiological pH.[10b] Our studies demonstrate that the electronic absorption spectrum of [Cu^{II}(PrP(106−114))] is nearly identical with the Cu^{II} adduct of full length fragment PrP(91−126) (λ_{max} = 604 nm (ϵ = 124 M^{-1} cm^{-1}); Figure 1). Also similar is the presence of a feature in the pH 7.4 CD spectrum of both [Cu^{II}(PrP(106−114))] and [Cu^{II}-(PrP(91−126))] that is consistent with a Met(S) → Cu^{II} ligand to metal charge-transfer band (LMCT) at ∼380 nm (Supporting Information). We note that this feature is observed as a poorly resolved shoulder in the electronic absorption spectra. This LMCT had also been observed using CD by Di Natale et al. for [Cu^{II}(PrP(106−114))] and was considered consistent with a Met(S)−Cu^{II} motif.[10b]

Gel permeation chromatography (GPC) (Figure 2) demonstrates that both [Cu^{II}(PrP(91−126))] and [Cu^{II}(PrP(106−114))] are monomeric in solution, confirming that there is no appreciable peptide aggregation or interpeptide Cu^{II} coordination occurring. For [Cu^{II}(PrP(91−126))] the GPC derived molecular weight is 3480 Da (calcd: 3545 Da) while

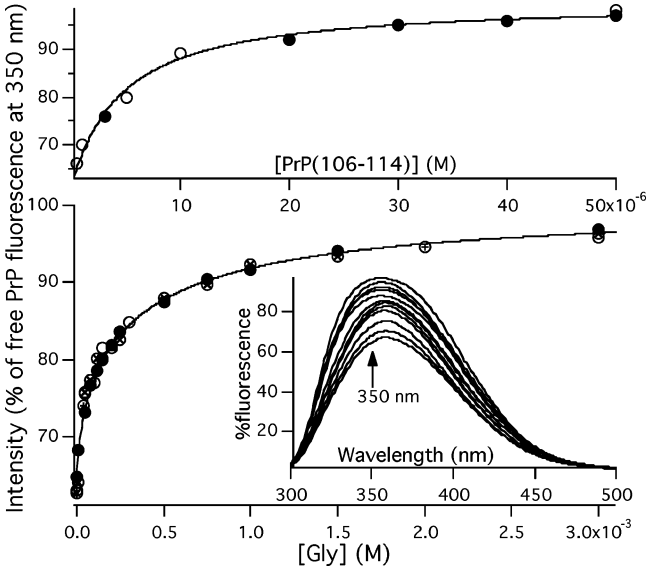

Figure 3. Titration curves used to determine Cu^{II} dissociation constants from [Cu^{II}(PrP(91−126))] and [Cu^{II}(PrP106−114))] by monitoring the increase in the W emission at 350 nm (inset) (pH 7.4; 50 mM NEM). The bottom curve depicts the competitive Cu^{II} binding of glycine added to solutions of [Cu^{II}(PrP(91−126))], and the top depicts the competitive Cu^{II} binding of PrP(106−114) added to solutions of [Cu^{II}(PrP(91−126))]. The open, closed, and dotted circles represents data taken from different titration experiments. The solid lines represent best fits to the data using the procedure outlined above.

for [Cu^{II}(PrP(106−114))] the GPC derived molecular weight is 1210 Da (calcd: 1120 Da). These are both consistent for the molecular weights of the metallopeptides, especially considering the error in GPC measurements. We note that identical chromatograms are obtained if data are collected at λ = 350 nm (where the free peptide does not absorb) or λ = 254 nm, indicating we are observing the metallopeptide in the chromatograms.

Cu^{II} dissociation constants from [Cu^{II}(PrP(91−126))] were probed at pH 7.4 (50 mM NEM) by performing a competitive Cu^{II} binding experiment with glycine. If glycine is added to solutions of [Cu^{II}(PrP(91−126))] it will strip Cu^{II} from the metallopeptide forming Cu^{II}(glycine)$_2$. This process can be examined using fluorometry by monitoring the fluorescence of the W(99) emission at 350 nm upon excitation at 285 nm. As Cu^{II} coordinates to PrP(91−126) the fluorescence of the W residue is quenched to 62% the intensity of the free peptide. Titration of a large excess glycine into solutions of [Cu^{II}(PrP(91−126))] restores the fluorescence intensity of the free peptide (Figure 3, inset). Using the procedure outlined above a K_d for [Cu^{II}(PrP(91−126))] of 98(2) μM is obtained (Figure 3, bottom plot), which is in line with studies performed by Viles and co-workers demonstrating excess glycine can remove Cu^{II} from [Cu^{II}(PrP(91−115))] at pH 7.5.[10d,20] Once the K_d was calculated for [Cu^{II}(PrP(91−126))] the K_d for [Cu^{II}(PrP(106−114))] could be determined. Using a procedure identical with that above (except PrP(106−114) is utilized in place of glycine as a the competitive Cu^{II} ligand) a K_d for [Cu^{II}(PrP(106−114))] of 86(10) μM is obtained (Figure 3, top plot). Our electronic absorption and Cu^{II} binding studies therefore suggest similar Cu^{II} coordination environments and Cu^{II} affinities for [Cu^{II}(PrP(106−114))]

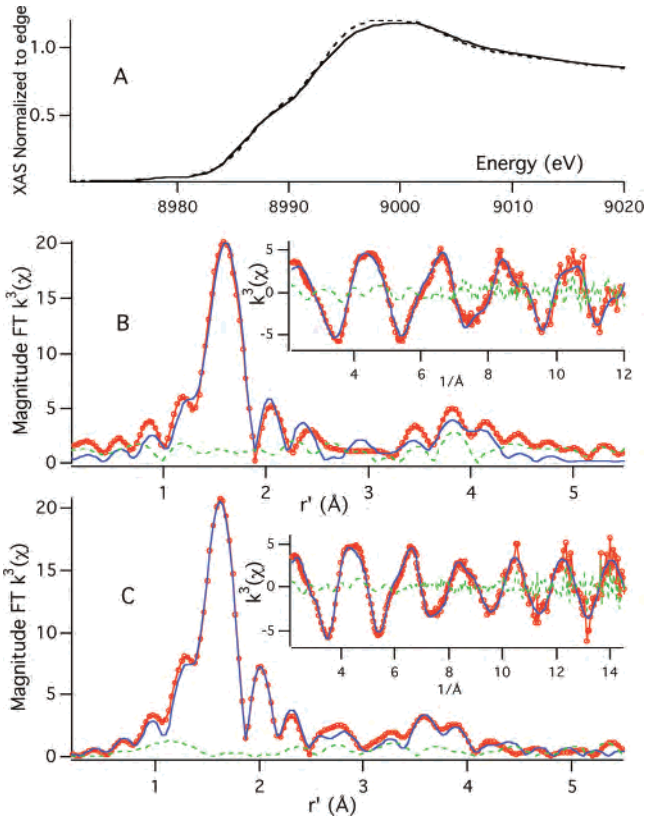

Figure 4. (A) Comparison of the edge region from the Cu K-edge XAS for [Cu^{II}(PrP(106−114))] (solid line) and [Cu^{II}(PrP(91−126))] (dashed line). The bottom figures depict the k^3 and magnitude FT k^3 EXAFS for (B) [Cu^{II}(PrP(91−126))] and (C) [Cu^{II}(PrP(106−114))]. The data are presented as connected red circles, the best fits are the solid blue lines, and the difference spectra are the dashed green lines. All data were recorded at 20 K (pH 7.4 in 50 mM NEM buffer).

vs [Cu^{II}(PrP(91−126))] exist. We probed this further using X-ray absorption spectroscopy (XAS).

XAS Studies of [Cu^{II}(PrP(91−126))] and [Cu^{II}(PrP(106−114))]. The preedge region of the Cu K-edge spectra for both of these metallopeptides reveals a weak transition at 8979 eV assigned to the 1s → 3d transition, and a shoulder at 8987 eV assigned to a 1s → 4p + LMCT transition (Figure 4a).[21] The intensities of the transitions and edge shapes produced by both metallopeptides are virtually identical indicating similar Cu^{II} coordination environments. The EXAFS region of the Cu K-edge spectrum also demonstrates the similarities in Cu coordination environments for these metallopeptides (Figure 4b,c). [Cu^{II}(PrP(106−114))] was best modeled with copper in an N_3S coordination environment with 2 nitrogen scatterers at 1.965(2) Å, 1 sulfur scatterer at 2.301(6) Å, and 1 imidazole scatterer at 1.979(7) Å (Table 1). Although the Cu−S distance is somewhat short for a Cu^{II}−thioether bond, it is not without precedent.[22] Furthermore, most of the structurally characterized Cu^{II}−thioether complexes are five, not four coordinate, which will result in a lengthening of the Cu−S bond.

Table 1. XAS Refinement Parameters for the Most Statistically and Physically Significant Refinements Using [Cu^{II}(PrP(106−114))] and [Cu^{II}(PrP(91−126))]

param	[Cu^{II}(PrP(91−126))]	[Cu^{II}(PrP(106−114))]
preedge peak no. 1 (eV) (area (eV)	8979.2(5) (0.04(1))	8978.9(3) (0.035(7))
preedge peak no. 2 (eV) (area (eV)	8983.8(9) (0.08(3))	8983.0(4) (0.07(2))
E_o (eV)[a]	8988.7	8989.6
N shell		
n	2.0(2)	2.3(2)
r (Å)	1.976(3)	1.965(2)
σ^2 (Å^2)	0.0008(8)	0.0009(5)
S shell		
n	0.8(3)	0.7(2)
r (Å)	2.280(2)	2.301(6)
σ^2 (Å^2)	0.008(2)	0.006(3)
Im shell		
n	1.3(3)	1.2(2)
r (Å)	1.994(9)	1.979(7)
σ^2 (Å^2)	0.003(2)	0.002(2)
θ (deg)	8(4)	19(6)
ϕ (deg)	133(11)	131(13)
resolution[b] (Å)	0.16	0.13
GOF	1.12	0.76
BVS[c]	2.15	2.17

[a] For both refinements E_o was initially refined for the N shell and then restrained. [b] The resolution is the distance that two shells of similar type can be separated and be considered to be resolvable by EXAFS. It is related to the data quality at high k by resolution = $\pi/(2\Delta k)$. We consider the N and Im shells to be distinct because the Im shell contains information for both the inner-sphere N scatterer, outer-sphere C scatterers, and multiple scattering pathways. For this data Δk is 9.8 Å^{-1} for [Cu^{II}(PrP(91−126))] and 12.1 Å^{-1} for [Cu^{II}(PrP(106−114))]. [c] The values for the number of ligands were set to the nearest whole number.

It should also be noted that the inclusion of oxygen scatterers in place of the non-imidazole nitrogen scatterers gave slightly poorer fits to the data (see Supporting Information). However, the refinements are still physically reasonable and statistically valid. Therefore one or two oxygen-based Cu ligands (i.e., a carbonyl oxygen from the peptide backbone) cannot be completely ruled out on the basis of these data. However, we favor the formulation of nitrogen-based amide donors as ligands for Cu^{II} for several reasons. There is a strong pH dependence for Cu^{II} coordination to this segment of the PrP, with virtually no Cu^{II} coordination observed at low pH.[23] This suggests that the deprotonation of a ligand is necessary for copper coordination, consistent with amide ligation. Such a strong pH dependence for Cu^{II} coordination is also observed in the octarepeat domain, which provides two amide nitrogens from the peptide backbone as ligands for Cu^{II} at physiological pH.[9a] Furthermore, both EPR and ENDOR studies performed on the Cu^{II} adducts of the PrP with the octarepeat region deleted are consistent with non-imidazole-based nitrogen ligands coordinated to the Cu^{II} center consistent with nitrogen ligands from the peptide backbone.[10c,24]

(21) (a) DuBois, J. L.; Mukherjee, P.; Stack, T. D. P.; Hedman, B.; Solomon, E. I.; Hodgson, K. O. *J. Am. Chem. Soc.* **2000**, *122*, 5775−5787. (b) Kau, L.-S.; Spira-Solomon, D. J.; Penner-Hahn, J. E.; Hodgson, K. O.; Solomon, E. I. *J. Am. Chem. Soc.* **1987**, *109*, 6433−6442.

(22) (a) The average Cu^{II}−SR_2 bond length as of 1989 was 2.347(53) Å. The average was skewed toward longer Cu−S bonds with 25% of all Cu^{II}−SR_2 below 2.323 Å and 25% of all Cu^{II}−SR_2 above 2.390 Å: Orpen, A. G.; Brammer, L.; Allen, F. H.; Kennard, O.; Watson, D. G.' Taylor, R. *J. Chem. Soc., Dalton Trans.* **1989**, S1−S83. (b) For example, see the following: Flanagan, S.; Dong, J.; Haller, K.; Wang, S.; Scheidt, W. R.; Scott, R. A.; Webb, T. R.; Stanbury, D. M.; Wilson, L. J. *J. Am. Chem. Soc.* **1997**, *119*, 8857−8868.

(23) Whittal, R. M.; Ball, H. L.; Cohen, F. E.; Prusiner, S. B.; Baldwin, M. A. *Protein Sci.* **2000**, *9*, 332−343.

In the case of either nitrogen- or oxygen-based ligands, a four coordinate geometry is most consistent with a bond valence sum analysis (BVS).[15] A bond valence (s; eq 5) is an empirically derived quantity in which the experimentally determined bond lengths (r) are compared with some reference bond length for a particular metal ligand bond (r_o). Summing together the individual values for s yields the BVS. In the most widely utilized analysis the final BVS will ideally equal the oxidation of the metal complex. When we apply a BVS for four coordinate [Cu^{II}(PrP(106−114))] in either CuN_3S, CuN_2OS, or $CuNO_2S$ ligand environments, the BVS spans between 1.92 and 2.17, which are reasonable for four coordinate Cu^{II}. Utilizing a five coordinate Cu^{II} coordination environment causes the BVS to increase to 2.78−3.33, strongly arguing against a five coordinate ligation scheme. Attempts to refine the EXAFS data as a six coordinate copper center did not yield a physically reasonable model.

Similar to the simulations of the EXAFS data for [Cu^{II}-(PrP(106−114))] the EXAFS data for [Cu^{II}(PrP(91−126))] were best modeled with Cu^{II} contained in an $(N/O)_3S$ ligand environment with virtually identical structural parameters (2 N/O at 1.976(3) Å; 1 S at 2.280(2) Å; 1 imidazole at 1.994-(9) Å; Table 1). A BVS analysis for [Cu^{II}(PrP(91−126))] using a the four coordinate $Cu(N/O)_3S$ models yields a range 2.05−2.15. This strongly suggests that the physiologically relevant high-affinity Cu^{II} binding region within the amyloidogenic PrP fragment is contained between residues 106 and 114. Also considering the similarities in coordination environment for the two metallopeptides, these data also seem to indicate that [Cu^{II}(PrP(106−114))] will make a good structural model for the relatively insoluble Cu^{II} adduct of PrP(91−126).

In a previous EXAFS study six coordinate Cu^{II} was proposed as the relevant coordination geometry within this region of the PrP,[10a] which we do not agree with for several reasons. First we calculate a BVS = 2.3 from the data provided in the previous EXAFS study, which is somewhat high for Cu^{II}. We also find that a six coordinate Cu^{II} is inconsistent with our edge data, EXAFS refinements, and BVS analysis, all of which suggests Cu^{II} is contained within a four coordinate square planar coordination geometry. Furthermore Millhauser,[10c] Viles,[10d] and Rizzarelli[10b] have all observed that square planar Cu is most consistent with the EPR spectra of various Cu^{II} metallopeptides derived from the amyloidogenic PrP segment over a wide range of pH. In a recent study by Di Natale et al., a CuN_3S coordination mode for [Cu^{II}(PrP(106−114))] at pH = 7.4 was proposed on the basis of electronic absorption and CD data.[10b] We note that the study by Di Natale et al. also suggested that the CuN_3S coordination mode may be in equilibrium with a CuN_4 species. Although our EXAFS analysis is consistent with the CuN_3S structure, we cannot rule out a minor contribution from a CuN_4 species.

Electrochemistry of Immobilized Films of [Cu^{II}(PrP-(106−114))] and [Cu^{II}(PrP(91−126))]. We next examined both [Cu^{II}(PrP(91−126))] and [Cu^{II}(PrP(106−114))] electrochemically as immobilized films on Pt electrodes at pH = 7.4 to determine if either metallopeptide is redox active and has a physiologically accessible redox potential. Thin films of [Cu^{II}(PrP(106−114))] and [Cu^{II}(PrP(91−126))] were prepared by the methods of Rusling et al.[16] A surfactant bilayer of *N*,*N*-dimethyldidodecylammonium bromide (DDAB) was formed on a freshly polished Pt electrode. The electrode was then placed in a solution of metallopeptide at pH = 7.4 for approximately 30 min by which time the metallopeptide had become incorporated into the DDAB film. Prepared in such a way we could store the metallopeptide on the electrode surface for several weeks and not observe any change in the electrochemical behavior of the films. We note that attempts to prepare immobilized films of these metallopeptides with coadsorbants such as neomycin or polymyxin were unsuccessful.

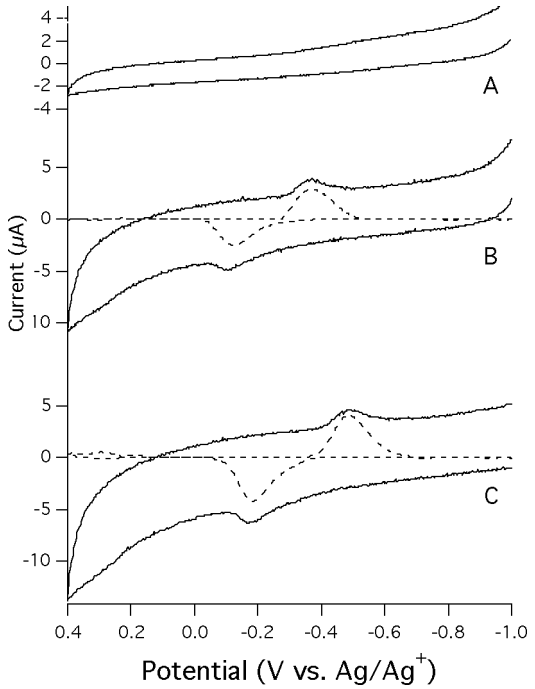

Figure 5. Cyclic voltammograms of DDAB bilayers of (B) [Cu^{II}(PrP-(91−126)] and (C) [Cu^{II}(PrP(106−114))] obtained at scan rates of 100 mV/s in Ar-purged water (pH = 7.4, 100 mM NaCl). The dashed lines represent the data (×3) with the background current removed. The top CV (A) displays the electrochemical response of the bilayer with no metallopeptide incorporated into it.

Figure 5 displays typical cyclic voltammograms (CVs) obtained from [Cu^{II}(PrP(91−126))] and [Cu^{II}(PrP(106−114))] contained within the DDAB bilayers at a scan rate of 100 mV/s under strict anaerobic conditions. Both display quasireversible behavior for the Cu^{II}/Cu^{I} redox couple with an $E_{1/2}$ = −0.33 V vs Ag/AgCl for [Cu^{II}(PrP(106−114))] and −0.35 V vs Ag/AgCl for [Cu^{II}(PrP(91−126))]. The peak widths at half-height (87(2) mV for [Cu^{II}(PrP(106−114))] and 91(4) mV for [Cu^{II}(PrP(91−126))]) are both consistent with 1 e^- redox processes.[17] Large peak separations at this scan rate are obtained for both metallopeptides (E_p = 0.2−0.3 V compared to ∼20 mV for fully reversible immobilized species), which suggests a relatively large structural rearrangement upon Cu reduction/oxidation. This is consistent

(24) Van Doorslaer, S.; Cereghetti, G. M.; Glockshuber, R.; Schweiger, A. *J. Phys. Chem. B* **2001**, *105*, 1631−1639.

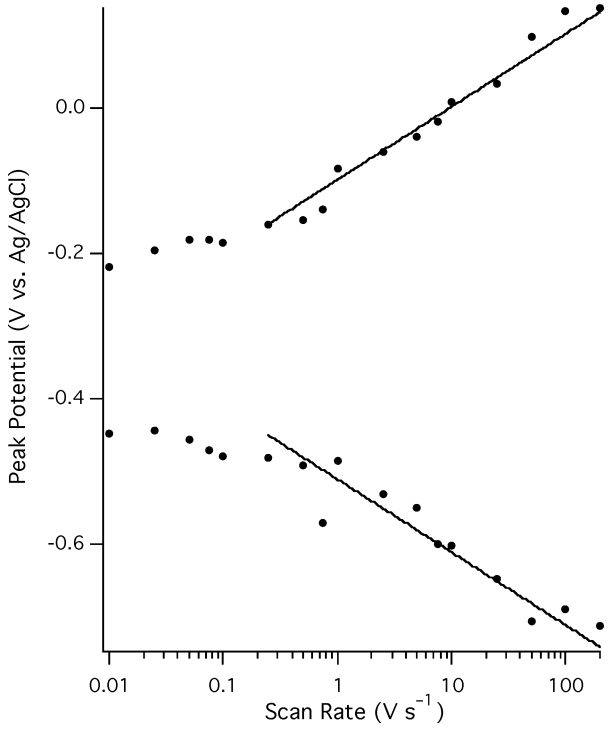

Figure 6. Variation in peak potential as a function of scan rate for [Cu^{II}(PrP(106−114))]. The solid lines represent best fits to the data using eqs 7 and 8.

with a Cu^{II}/Cu^{I} redox process, where a change in coordination geometry should be expected.[25] Also consistent with a Cu^{II}/Cu^{I} redox process is the relatively slow standard average rate constant for ET (k_o, Figure 6).[25] Laviron's procedure[18a] was utilized for the calculation of k_o by measuring the change in peak position as a function of scan rate. Application of eqs 7 and 8 yielded average $k_o = 0.2(1)$ s^{-1} for the oxidation and reduction processes of immobilized film of [Cu^{II}(PrP(106−114))] (0.11(1) s^{-1} for the oxidation process and 0.36(7) s^{-1} for the reduction process). If dioxygen is introduced into the electrochemical solution, a catalytic current is produced indicating that O_2 is being catalytically reduced (Supporting Information). These results strongly suggest that the Cu^{I} adduct of both PrP(106−114) and PrP(91−126) should be stable under physiological conditions and that each can be prepared through the use of a biologically relevant reductant.

Cu^{I} Adduct of PrP(106−114) and PrP(91−126). The electrochemical data suggested that both [Cu^{II}(PrP(106−114))] and [Cu^{II}(PrP(91−126))] are redox active under physiological conditions. We therefore explored the reaction between [Cu^{II}(PrP(106−114))] and [Cu^{II}(PrP(91−126))] with a biologically relevant reductant, ascorbate. Introduction of an excess of ascorbic acid into anaerobic solutions of either [Cu^{II}(PrP(106−114))] or [Cu^{II}(PrP(91−126))] (pH = 7.4; 50 mM NEM) leads to an immediate bleaching of the solution indicating the reduction of the blue Cu^{II} metallopeptides to their colorless Cu^{I} adducts. ESI-MS data obtained for these solutions indicates that Cu^{I} is coordinating to both PrP(91−126) and PrP(106−114) (see Supporting Information).

(25) Rorabacher, D. B. *Chem. Rev.* **2004**, *104*, 651−698.

Table 2. XAS Refinement Parameters for the Most Statistically and Physically Significant Refinements Using [Cu^{I}(PrP(106−114))] and [Cu^{I}(PrP(91−126))]

param	[Cu^{I}(PrP(91−126))]	[Cu^{I}(PrP(106−114))]
preedge peak (eV) (area (eV)	8991(1) (0.16(1))	8986(1) (0.35(1))
E_o (eV)[a]	8988.3	8987.5
N shell		
n	1.7(2)	0.7(1)
r (Å)	2.048(4)	2.057(6)
σ^2 (Å^2)	0.0037(3)	0.0018(9)
S shell		
n	1.9(1)	2.3(2)
r (Å)	2.313(2)	2.358(2)
σ^2 (Å^2)	0.0029(3)	0.0022(3)
N/O shell		
n		1.3(2)
r (Å)		2.159(3)
σ^2 (Å^2)		0.0018[b]
resolution[c] (Å)	0.16	0.13
GOF	0.82	0.45
BVS[d]	0.83	1.08

[a] For both refinements E_o was initially refined for the N shell and then restrained. [b] We restrained σ^2 in this shell to be equal to the inner-sphere nitrogen shell. Refinement of this parameter produced a negative value for σ^2, which is physically impossible. [c] The resolution is the distance that two shells of similar type can be separated and be considered to be resolvable by EXAFS. It is related to the data quality at high *k* by resolution = $\pi/(2\Delta k)$. [d] The value for the number of ligand was set to the nearest whole number.

Introduction of dioxygen into solutions of either [Cu^{I}(PrP(106−114))] or [Cu^{I}(PrP(91−126))] leads to the rapid oxidation of the metallopeptides reproducing [Cu^{II}(PrP(106−114))] or [Cu^{II}(PrP(91−126))]. This provides further evidence of the reversibility of the Cu^{II}/Cu^{I} redox processes for these metallopeptides. We therefore investigated the structure of the Cu^{I} adducts of PrP(91−126) and PrP(106−114) using Cu K-edge X-ray absorption spectroscopy (Table 2).

Figure 7a depicts the edge spectra of both metallopeptides. The position of the edge shifted to lower energies by ∼2−3 eV, which is consistent with a change in oxidation state from Cu^{II} to Cu^{I}. Also consistent with the reduction of Cu^{II} (d^9) to Cu^{I} (d^{10}) is the loss of the weak preedge feature corresponding to the 1s → 3d transition. Both spectra display a shoulder at ∼8987 eV that is ascribed to the 1s → 4p transition.[21b] This transition is more pronounced in [Cu^{I}(PrP(106−114))] than in [Cu^{I}(PrP(91−126))], which seems to indicate that the coordination environment in [Cu^{I}(PrP(91−126))] is more symmetric than in [Cu^{I}(PrP(106−114))]. Such a situation would lead to a higher degree of degeneracy in the Cu 4p orbitals and hence a "blurring" of the 1s → 4p transitions.[21b] Not only is this preedge feature significantly different in [Cu^{I}(PrP(106−114))] than in [Cu^{I}(PrP(91−126))] but the overall shape of the XANES is significantly different between the two metallopeptides. Considering that the XANES region is highly sensitive to the coordination environment about the metal center, this indicates that a differential coordination geometry most likely exists in these two Cu^{I} metallopeptides.

The EXAFS region of the X-ray absorption spectrum for [Cu^{I}(PrP(106−114))] (Figure 7c) was best modeled in a distorted CuN_2S_2 coordination environment by employing one Cu−N scatterers at 2.057(6) Å, one Cu−N scatterer at

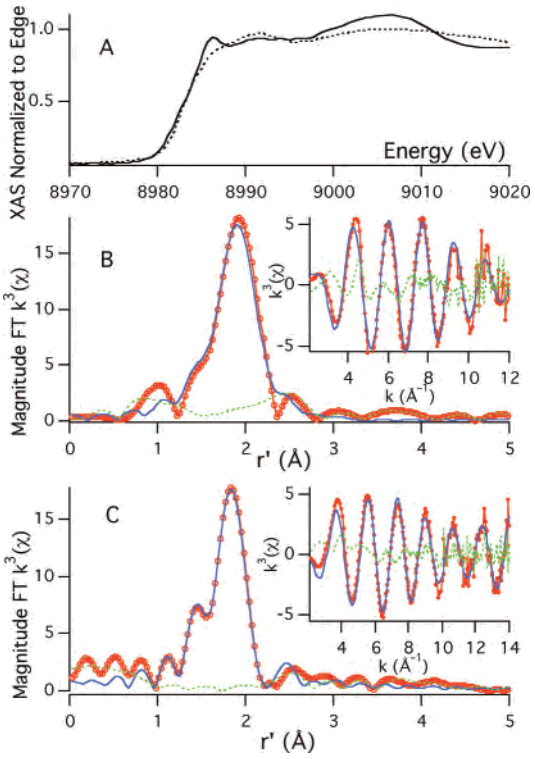

Figure 7. (A) Comparison of the edge region from the Cu K-edge XAS for ascorbate-reduced [Cu^{I}(PrP(106−114))] (solid line) and [Cu^{I}(PrP(91−126))] (dashed line). The bottom figures depict the k^3 and magnitude FT k^3 EXAFS for (B) [Cu^{I}(PrP(91−126))] and (C) [Cu^{I}(PrP(106−114))]. The data are presented as connected red circles, the best fits are the solid blue lines, and the difference spectra are the dashed green lines. All data were recorded at 20 K (pH 7.4 in 50 mM NEM buffer).

2.159(3) Å, and two Cu−S scatterers at 2.358(2) Å. The increase in the number of coordinated thioether ligands (which are soft bases) from 1 to 2 is consistent with the change in the hardness of the copper ion upon reduction of Cu^{II} (hard) to Cu^{I} (soft).

Although the difference in Cu−N distance between the two Cu−N shells is less than the minimum warranted by the resolution of our data (resolution = 0.13 Å), combining these two into one shell produced a poorer fit to the data (GOF = 0.45 vs 0.57). Furthermore, when the two nitrogen shells are merged into one the BVS parameter becomes inconsistent with Cu^{I} (vide infra). It was therefore decided to retain this shell in the final refinements to the data. Inclusion of the Im scatterer in these data refinements did not lead to a statistically better fit to the data or yield physically reasonable values for the corresponding in- and out-of plane bond angles. Therefore the Cu−Im scatterer was not used in the refinements to [Cu^{I}(PrP(106−114))] (or the ones for [Cu^{I}(PrP(91−126))]). This does not imply that Cu−His ligation is lost, merely that the imidazole moiety has either (1) become significantly disordered such that it cannot be reliably located based on the outer-sphere scatterers and MS pathways that define the Cu−Im function or (2) θ is larger than 50° and the MS pathways from the imidazole ligand do not contribute significantly to the EXAFS. Similar to the refinements reported above for [Cu^{II}(PrP(106−114))], we could substitute oxygen for nitrogen scatterers without a large impact on the resulting GOF. The BVS for four coordinate [Cu^{I}(PrP(106−114))] with Cu(N/O)(N/O)S$_2$ ligation ranged between 1.04 and 1.08, consistent with Cu^{I}. Merging the two N/O shells into one shell yielded a BVS between 0.49 and 0.64, significantly below the expected value of 1. We could not refine these data for a three or five coordinate model and obtain physically realistic refinement parameters (three coordinate) or an improved BVS (>1.3 for the five coordinate models).

As could be predicted from the edge data, the EXAFS analysis for [Cu^{I}(PrP(91−126))] (Figure 7b) also suggested a differential coordination environment compared to [Cu^{I}(PrP(106−114))]. The EXAFS data for [Cu^{I}(PrP(91−126))] could be modeled as a four coordinate copper center (Cu(N/O)$_2$S$_2$) with two Cu−N/O scatterers at 2.048(4) Å and two Cu−S scatterers at 2.313(2) Å. Such a situation would lead to a high-symmetry Cu^{I} center in [Cu^{I}(PrP(91−126))] vs [Cu^{I}(PrP(106−114))], which was suggested by the XANES analysis. Although these structural parameters are reasonable for Cu^{I}, we note that the resulting BVS is not fully consistent with Cu^{I}. The BVS values for the three possible four coordinate models (Cu(N/O)$_2$S$_2$) range from 0.74 to 0.83. Alternatively, the EXAFS data for [Cu^{I}(PrP(91−126))] could be modeled as a five coordinate (N/O)$_2$OS$_2$ Cu^{I} center with two Cu−N/O scatterers at 2.051(10) Å, two Cu−S scatterers at 2.301(2) Å, and one long Cu−O scatterer at 2.559(7) Å, which is essentially nonbonding (BVS = 0.99). Although the bond lengths and BVS are consistent with Cu^{I}, we note that a coordination number of 5 is not well established for Cu^{I}. Also, the long-range Cu−O interaction could easily be a misidentified outer-sphere carbon scatterer (from the peptide backbone). Therefore, we point out that the four coordinate model is more reasonable from a chemical point of view. At this point we cannot determine if the differences in coordination environment between [Cu^{I}(PrP(106−114))] and [Cu^{I}(PrP(91−126))] reflect the ligation of residues outside of the PrP(106−114) region in [Cu^{I}(PrP(91−126))] or if the different peptide microenvironments afforded by PrP(106−114) vs PrP(91−126) are influencing the coordination geometry.

Quantification of $O_2^{\bullet-}$ Produced by [Cu(PrP(106−114))] and [Cu(PrP(91−126))]. Our XAS analysis indicates that both PrP(106−114) and PrP(91−126) are capable of coordinating Cu^{I} in well-defined coordination environments, while electrochemical and electronic absorption studies indicate that these metallopeptides are capable of catalytically reducing dioxygen to superoxide ($O_2^{\bullet-}$). Not only has $O_2^{\bullet-}$ been implicated in many different diseases in humans[26] but it is also the initial intermediate produced in the formation of reactive oxygen species (ROSs) such as H_2O_2, singlet O_2, and $HO^{\bullet}$, all of which are highly toxic to cells.[27] These ROSs are also capable of performing oxidative modification to proteins, which could in turn lead to protein misfolding

(26) (a) Valentine, J. S.; Hart, P. J. *Proc. Natl. Acad. Sci. U.S.A.* **2003**, *100*, *3617*−3622. (b) Mendez-Alvarez, E.; Soto-Otero, R.; Hermida-Ameijeiras, A.; Lopez-Real, A. M.; Labandeira-Garcia, J. L. *Biochim. Biophys. Acta* **2002**, *1586*, *155*−168. (c) Jenner, P.; Olanow, C. W. *Ann. Neurol.* **1998**, *44*, S72−S84. (d) Kim, G. W.; Kondo, T.; Noshita, N.; Chan, P. H. *Stroke* **2002**, *33*, 809−815.
(27) Sawyer, D. T.; Valentine, J. S. *Acc. Chem. Res.* **1981**, *14*, 393−4400.

events.[28] We therefore examined if these metallopeptides are capable of producing $O_2^{\bullet-}$ utilizing a nitroblue tetrazolium (NBT) assay. NBT is a colorless compound that is reduced to the blue pigment formazan (ϵ_{520} ~35 000 M^{-1} cm^{-1})[29] upon exposure to $O_2^{\bullet-}$. In a typical reaction 0.5 mM [Cu^{II}(PrP(106−114))] or [Cu^{II}(PrP(91−126))] is added aerobically to a 100 mM solution of ascorbic acid and 0.035 mM NBT (pH = 7.4). This produced an immediate bleaching of the solution, which was followed by the gradual increase of a charge-transfer band at ~600 nm corresponding to formazan production. The increase in the band corresponding to formazan was then monitored (at 580 nm) over the course of several hours and was correlated to a steady-state production of ~0.3 mmol dm^{-1} min^{-1} for both metallopeptides.[30] This suggests that the differential Cu^I coordination environments found within the two metallopeptides are having a minimal influence of $O_2^{\bullet-}$ production. We note that the NBT/formazan assay performed under identical conditions with either $CuCl_2$ or [Cu^{II}(PrP(61−65))] (an octarepeat mimic)[13,31] used in place of [Cu(PrP(106−114))] or [Cu(PrP(91−126))] indicates that $O_2^{\bullet-}$ is not produced with these copper sources.

Summary and Biological Relevance. In this report we have demonstrated that the minimal PrP fragment required for the coordination of Cu^{II} in a manner nearly identical with the neurotoxic PrP fragment most likely lies between residues 106 and 114. This is consistent with studies recently reported by Viles,[9] which suggested that residues around H(96) were not involved in coordinating Cu within a "high-affinity site." From our EXAFS analysis both [Cu^{II}(PrP(106−114))] and [Cu^{II}(PrP(91−126))] contain copper in a square planar coordination environment with three N/O ligands (one of which is derived from His) and one Met thioether ligand. Both metallopeptides are redox active, displaying quasireversible $Cu^{II/I}$ redox potentials at ~−0.3 V vs Ag/AgCl. Upon reduction of the copper center with ascorbate, both produce stable Cu^I centers in well-defined coordination environments. Both [Cu^I(PrP(106−114))] and [Cu^I(PrP(91−126))] are most likely four coordinate with two N/O ligands and two thioether ligands.

An important findings of this study from a biological perspective is that upon reduction to Cu^I both metallopeptides can produce the ROS $O_2^{\bullet-}$. First we feel that these data provide additional evidence for eliminating one possible role of the PrP, that of a superoxide dismutase (SOD).[12a] These data show that the Cu^I/Cu^{II} redox potential for the copper adduct of the neurotoxic PrP fragment lies outside of the range that would allow it to act as an SOD.[32] Furthermore, the copper adduct of the neurotoxic PrP fragment produces $O_2^{\bullet-}$ as opposed to catalytically disproportionating it. Coupled with the redox inactivity of Cu^{II} contained in the octarepeat domain we find it unlikely that the PrP behaves as an SOD. Another consequence of this work involves the potential prion disease mechanism. These results demonstrate that a metal-mediated oxidative damage mechanism is *in theory* possible for prion disease since both of these PrP-derived metallopeptides can produce the toxic one-electron-reduced dioxygen product $O_2^{\bullet-}$.[5b] It remains to be seen if $O_2^{\bullet-}$ or other ROS production from these copper−PrP adducts occurs in vivo.

Acknowledgment. We thank the University of Nevada, Reno, NV, for financial support. We also thank Prof. H.-J. Woo (UNR) for performing some molecular dynamics simulations. XAS data were recorded at the NSLS (Brookhaven National Laboratories, Upton, NY) under U.S. DOE Contract No. DE-AC02-98CH10886.

Supporting Information Available: ESI-MS data for [Cu^I(PrP(91−126))] and [Cu^I(PrP(106−114))], NBT/formazan assay results, CV of [Cu^{II}(PrP(106−114))] indicating catalytic O_2 reduction, alternative refinements of the EXFAS data for the metallopeptides, pH 7.4 CD spectra of [Cu^{II}(PrP(91−126))] and [Cu^{II}(PrP(106−114))], a pH 7.4 high-energy electronic absorption spectrum of [Cu^{II}(PrP(106−114))], and coordinates for the Cu-metallopeptide fragment used to derive the Cu−Im function. This material is available free of charge via the Internet at http://pubs.acs.org.

IC061236S

(28) Niki, E. *Free Radical Res.* **2000**, *33*, 693−704.
(29) Bielski, H. J.; Shiuw, G. G.; Bajuk, S. J. *J. Phys. Chem.* **1980**, *84*, 830.
(30) Tabbi, G.; Driessen, W. L.; Reedijk, J.; Bonomo, R. P.; Veldman, N., Spek, A. L. *Inorg. Chem.* **1997**, *36*, 1168−1175.
(31) Burns, C. S.; Aronoff-Spencer, E.; Dunham, C. M.; Lario, P.; Avdievich, N. I.; Antholine, W. E.; Olmstead, M. M.; Vrielink, A.; Gerfen, G. J.; Peisach, J.; Scott, W. G.; Millhauser, G. L. *Biochemistry* **2002**, *41*, 3991−4001.
(32) (a) Miller, A.-F. *Curr. Opin. Chem. Biol.* **2004**, *8*, 162−168. (b) Fridovich, I. *Encycl. Biol. Chem.* **2004**, *4*, 135−138.